Method for determining kinematic parameters of the *in vivo* thumb carpometacarpal joint

Lillian Y. Chang *Student Member, IEEE,* and Nancy S. Pollard *Member, IEEE*

Abstract—The mobility of the thumb carpometacarpal (CMC) joint is critical for functional grasping and manipulation tasks. We present an optimization technique for determining from surface marker measurements a subject-specific kinematic model of the *in vivo* CMC joint that is suitable for measuring mobility. Our anatomy-based cost metric scores a candidate joint model by the plausibility of the corresponding joint angle values and kinematic parameters rather than only the marker trajectory reconstruction error. The proposed method repeatably determines CMC joint models with anatomically-plausible directions for the two dominant rotational axes and a lesser range of motion (RoM) for the third rotational axis. We formulate a low-dimensional parameterization of the optimization domain by first solving for joint axis orientation variables which then constrain the search for the joint axis location variables. Individual CMC joint models were determined for 24 subjects. The directions of the flexion-extension (FE) axis and adduction-abduction (AA) axis deviated on average by 9 degrees and 22 degrees, respectively, from the mean axis direction. The average RoM for FE, AA, and pronation-supination (PS) joint angles are 76, 43, and 23 degrees for active CMC movement. The mean separation distance between the FE and AA axes was 4.6 mm, and the mean skew angle was 87 degrees from the positive flexion axis to the positive abduction axis.

Index Terms—subject-specific joint models, axes of rotation, optimization, thumb mobility

I. INTRODUCTION

THE mobility of the human thumb is a critical component of the hand's ability to grasp and manipulate objects. Subject-specific models can lead to more accurate evaluation of individual thumb motion and dynamic function. In this work we concentrate on the carpometacarpal (CMC) joint at the base of the thumb between the trapezium bone and metacarpal bone, which is responsible for the wide range of thumb circumduction and opposition [1, 2]. Determining appropriate, subject-specific models of this joint is important for evaluating individual thumb mobility with respect to the appropriate joint axes and creating customized hand models for virtual rehabilitation environments.

L. Y. Chang is with the School of Computer Science, Carnegie Mellon University, 5000 Forbes Ave., Pittsburgh, PA 15213, USA (email: lillianc@ri.cmu.edu)

N. S. Pollard is with the School of Computer Science, Carnegie Mellon University, 5000 Forbes Ave., Pittsburgh, PA 15213, USA (email: nsp@cs.cmu.edu)

Previous work by Hollister et al. [3] located the anatomic rotational axes of the *in vitro* CMC joint, and further studies by Santos and Valero-Cuevas [4] simulated possible kinematic models based on distributions of joint parameters from cadaveric measurement. Cooney et al. [5] also determined the orientation of *in vitro* CMC axes from the ridges of the trapezium bone surface in cadaver hands, and these results reported with respect to the hand dorsum provide a single constant model of the axis orientations to subsequently measure *in vivo* CMC mobility. Non-invasive techniques proposed by Coert et al. [6] and Zhang et al. [7] evaluate thumb circumduction based on the observed motion of the thumb segments, without determining a kinematic model for the thumb joints. In contrast, Chèze et al. [8] and Cerveri et al. [9] have developed techniques for estimation of the *in vivo* CMC axes from isolated thumb movements such as circumduction and flexion-extension. Our technique uses the entire joint range of motion (RoM) to determine an individual *in vivo* CMC joint model with two dominant rotational axes that are non-intersecting and non-orthogonal. The method accommodates any general surface marker protocol and can be used to measure joint RoM with respect to the subject-specific model fit to an individual's particular pattern of motion.

Several kinematic models have been used to describe the thumb CMC joint [3, 5, 10, 11]. The CMC joint motion is dominated by two degrees of freedom (DoFs) of flexion-extension (FE) and adduction-abduction (AA) and exhibits a lesser amount of pronation-supination (PS) [1, 5]. The simplest models [5, 10, 12] consider these axes intersecting and orthogonal, as part of either a two-DoF universal joint or a three-DoF spherical joint. However, the anatomy of the interfacing bone surfaces of the trapezium and thumb metacarpal bones suggests a saddle joint model with two axes that are non-intersecting and non-orthogonal (skew) [1, 3, 13], and this has been incorporated in a five-virtual-link thumb model for simulation [4, 11].

We use a three-DoF CMC joint model with non-intersecting FE and AA axes whose relative skew is determined by rotation about the PS axis. This model incorporates the complexity of the non-intersecting and non-orthogonal axes of the CMC saddle joint as in previous two-DoF models [3, 4, 11] while also allowing measurement of the PS rotation as the third DoF. Our approach optimizes an individual CMC joint model over a low-dimensional parameter space by decomposing the joint model into the two parts of joint axis orientation and joint axis location. The cost metric for the optimization scores anatomical characteristics of the CMC joint motion rather than only evaluating the marker trajectory reconstruction error as

used previously for similar joint models [14–16]. We find that to achieve subject-specific models of the CMC joint which also have anatomically-meaningful joint properties, minimizing the reconstruction error is insufficient because it leads to inconsistent estimates of axis directions and large RoM for the non-dominant DoF. Instead, optimizing our proposed metric determines a joint model which has anatomically-meaningful joint properties such as the relative RoM between the DoFs and the proximal-distal relative location of the axes.

II. METHOD

A. Experimental protocol

The study involved a total of 24 able-bodied individuals, consisting of 12 male (11 right-hand dominant, 1 left-hand dominant) and 12 female (11 right-hand dominant, 1 left-hand dominant) subjects, aged 26 ± 3.2 years (mean $\pm$ standard deviation). A Vicon camera system tracked the positions of reflective surface markers attached to the hand dorsum and thumb metacarpal segment, which defined the hand technical coordinate system (TCS) and thumb metacarpal TCS (Fig. 1a). Markers H1, H2, and H3 define the hand dorsum TCS and are attached, respectively, to the proximal end of the third metacarpal, the distal end of the third metacarpal, and the distal end of the second metacarpal. Markers T1, T2, and T3 define the thumb metacarpal TCS and are attached, respectively, to the proximal end of the first metacarpal on the ulnar side, the distal end of the first metacarpal on the ulnar side, and the distal end of the first metacarpal on the radial side. The marker locations were chosen to be spread out over the metacarpals of the hand dorsum and thumb to avoid, to the extent possible, large changes in the TCS orientation due to skin motion over the bone.

Subjects were seated at a table with the arm comfortably extended and the ulnar part of the hand in contact with the table surface for the data acquisition session (Fig. 1b). The calibration movement for sampling the full space of CMC joint configurations consisted of circumduction, a star pattern, abduction-adduction, and flexion-extension motions (Fig. 2). Subjects were directed to avoid motion of the other joints of the thumb, palm, and fingers, although these joints were not mechanically-constrained in order to encourage natural motion of the CMC joint. Subjects performed the calibration movement at a self-selected speed to exercise the active RoM of the CMC joint without any external contact to the thumb. Two repetitions of the movement pattern were recorded. The experiment was completed for both the right hand and left hand of each subject.

The recorded marker trajectories were lightly conditioned before use as input data as follows. Segments of static poses were manually clipped from the beginning and end of each motion sequence. In addition, any time samples with occluded markers were discarded. The resultant data sequence for one repetition of the calibration movement had on average 4500 time samples. For each of these remaining time samples, we computed the measured rigid transform A_m of the thumb metacarpal TCS with respect to the hand dorsum TCS (Fig. 3a), which consists of the relative orientation matrix R_m between the TCS axes and the position p_m of the metacarpal TCS
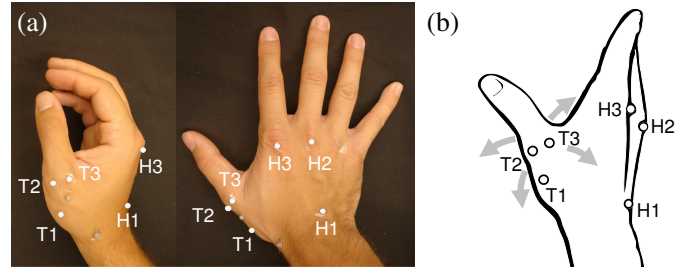
Fig. 1. (a) Marker protocol for the right hand used to measure the motion of the CMC joint in the experimental validation. Markers H1, H2, and H3 define the TCS for the hand dorsum, and markers T1, T2, and T3 define the TCS of the thumb metacarpal segment. A symmetric placement of markers was used for the left hand. The same marker protocol was used for all subjects to facilitate comparisons of the CMC axes locations, but the method can accommodate an arbitrary choice of the hand dorsum TCS and thumb metacarpal TCS. (b) Active RoM was measured while the subject exercised the CMC joint without any contact to the thumb.
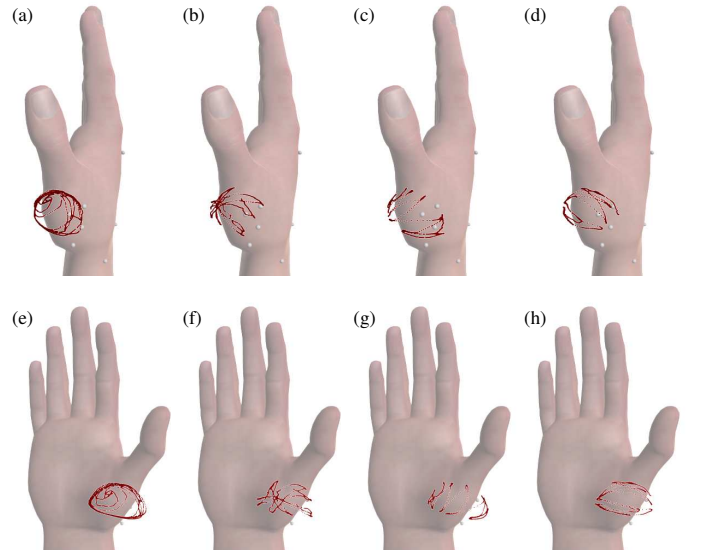
Fig. 2. An example of the calibration motion pattern measured from one subject. The trajectory of the T2 marker for the four portions of the motion pattern segment are shown for both radial and palmar views of the hand. (a,e) Clockwise and counter-clockwise circumduction. (b,f) A star pattern with arcs across the joint range of motion in multiple directions. (c,g) Zig-zag pattern with high-frequency adduction-abduction while gradually changing the flexion-extension angle. (d,h) Zig-zag pattern with high-frequency flexion-extension while gradually changing the adduction-abduction angle.

origin in the hand TCS frame. In addition, since the selection of the origin marker for the metacarpal TCS is arbitrary, our available data includes the positions (p_{m1}, p_{m2}, p_{m3}) of all three metacarpal markers in the hand TCS frame.

B. Problem statement

Given the sequence of measured relative TCS transforms A_m and marker positions (p_{m1}, p_{m2}, p_{m3}) from the data acquisition, we wish to determine the joint model which describes the orientation and location of the functional CMC rotational axes. In our model of the CMC joint (Fig. 3b), the joint angles θ_1, θ_2, and θ_3 denote three sequential rotations about the FE axis z_h, the PS axis, and the AA axis z_t, respectively. The FE axis z_h is the z-axis of the hand dorsum
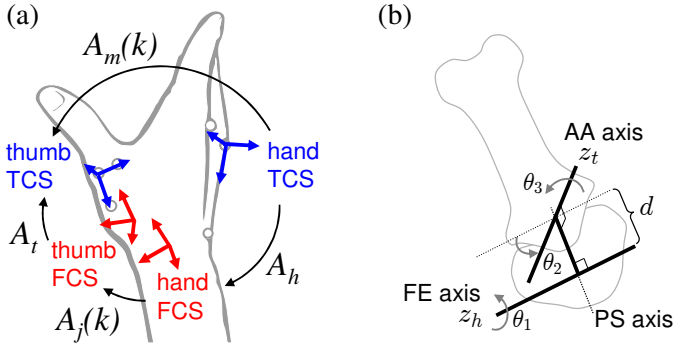
Fig. 3. (a) Technical coordinate systems (TCS) and functional coordinate systems (FCS) define the hand dorsum and thumb metacarpal segments adjacent to the CMC joint. The transform $A_m(k)$ describing the measured configuration of the CMC joint at time instance k is the composition of the change-of-coordinate transform A_h, the CMC configuration expressed relative to functional coordinate systems $A_j(k)$, and the change-of-coordinate transform A_t. (b) Model of the three rotational axes of the CMC saddle joint. The FE axis z_h is the z-axis of the hand dorsum FCS and is located through the trapezium bone. The AA axis z_t is the z-axis of the thumb metacarpal bone FCS. The FE and AA axes are separated by distance d along their mutual perpendicular which is the PS axis. The skew between the FE and AA axes is defined by the rotation angle θ_2 about the PS axis.

functional coordinate system (FCS), and the AA axis z_t is the z-axis of the thumb metacarpal FCS. The FE and AA axes are separated by a distance d along the PS axis, and the value of the PS rotation angle determines the skew between the FE axis and AA axis. For a complete description of the joint model, we need to solve for the hand dorsum FCS and thumb metacarpal FCS (Fig. 3a) which express the CMC movement in terms of functional FE, AA, and PS joint angles. We also need to solve for the constant separation d between the dominant FE and AA axes.

C. Optimization cost metric

To determine the joint model for an individual subject, we will use an optimization approach to select an appropriate set of hand FCS, thumb FCS, and separation d which result in rotational DoFs θ_1, θ_2, and θ_3 that both reconstruct the joint orientation and correspond to anatomically-meaningful FE, AA, and PS joint angles. We design our optimization cost metric for scoring candidate models as a combination of three cost components based on anatomical knowledge of the thumb CMC joint. The first aspect of the CMC joint motion is that it is dominated by FE and AA rotation with a limited amount of PS rotation, as reflected by the two-DoF models used in previous work [4, 11]. Thus the functional joint axes should correspond to joint variable sequences with small variation of θ_2 values. The second aspect is that the FE RoM is generally larger than the AA RoM for unimpaired CMC joints [5, 6]. Finally, the FE axis fixed in the hand frame is proximal to the AA axis fixed in the thumb metacarpal frame due to the saddle joint geometry between the metacarpal and trapezium bones [3, 4, 11, 13]. These three anatomical aspects of the CMC joint kinematics are incorporated into an overall cost metric which is minimized to solve for meaningful joint axes. All three components are used simultaneously since a single

component alone is not sufficient to satisfy all three objectives.

$$f = f_{PS} + f_{RoM} + f_d \tag{1}$$

The component f_{PS} reflects the property that the observed PS angle values should have small variation as the non-dominant rotational freedom. We motivate this cost metric component by a probabilistic model which assumes that the PS angle values are normally-distributed with mean value μ_2 and variance σ_2^2. To maximize the probability of observing a sequence of θ_2 values, we can equivalently minimize the corresponding negative log likelihood function of the modeled normal distribution, normalized by the sequence length N [see, e.g., 17]. This is used as one component of the cost metric:

$$f_{PS} = \frac{\sum_{k=1}^{N} (\theta_2(k) - \mu_2)^2}{2N\sigma_2^2} \tag{2}$$

where k indicates a single time sample in the sequence.

Since the absolute value of the angle is irrelevant for describing the overall amount of PS rotation, there is no prior set for μ_2 and we instead use the sample mean of the joint angle sequence,

$$\mu_2 = \frac{1}{N} \sum_{k=1}^{N} \theta_2(k). \tag{3}$$

The resultant form of Eq. (2) can be interpreted as the sample variance of the θ_2 values, scaled by a weighting factor $2\sigma_2^2$.

Next, the minimizing cost metric favors joint axis orientations which are aligned such that the FE RoM is maximized relative to the AA RoM:

$$f_{RoM} = \frac{range(\theta_3)}{range(\theta_1)} \tag{4}$$

where

$$range(\theta_i) = \max_{k \in (1,N)} (\theta_i(k)) - \min_{k \in (1,N)} (\theta_i(k)). \tag{5}$$

The final cost component measures how meaningful the estimated constant separation d is with respect to an assumed normal distribution with mean μ_d and variance σ_d^2. As before, maximizing the probability of the estimated separation d is equivalent to minimizing the negative log likelihood of d.

$$f_d = \frac{(d - \mu_d)^2}{2\sigma_d^2} \tag{6}$$

In this case, μ_d and σ_d provide intuitive weighting parameters which represent our prior belief in the possible values for anatomically-plausible separation distances. Selecting $\mu_d \geq 0$ represents the choice to favor CMC joint models where the FE axis is proximal to the AA axis, to be consistent with the CMC bone anatomy.

The overall optimization cost metric,

$$f = \frac{\sum_{k=1}^{N} (\theta_2(k) - \mu_2)^2}{2N\sigma_2^2} + \frac{range(\theta_3)}{range(\theta_1)} + \frac{(d - \mu_d)^2}{2\sigma_d^2}, \tag{7}$$

evaluates how well a candidate joint model corresponds to a meaningful decomposition of joint angles with an appropriate separation distance between the FE and AA axes. The three tuning parameters $(\sigma_2, \mu_d, \sigma_d)$ are used to adjust the relative

weights of the three unitless components f_{PS}, f_{RoM}, and f_d. The first component locates the direction of the PS axis with small variation in θ_2 values, the second component serves to distinguish between FE and AA directions according to the RoM ratio, and the third component selects models with appropriate separation distances.

D. Computation of joint parameters

In our optimization approach, we search the domain of candidate joint models for the joint model with minimum cost according to the anatomy-based cost metric in Eq. (7). In this section, we present how to formulate the optimization domain as the four-DoF set (z_h, z_t) specifying the orientations of the FE and AA axes. Then, given a measured data sequence and a candidate set (z_h, z_t), we can directly compute the remaining kinematic parameters and joint variables which are needed to evaluate the value of the cost metric. Pseudocode for the entire cost metric computation can be found in Fig. 4.

1) Kinematic model: At any time sample k, the measured CMC joint configuration $A_m(k)$ is related to the functional joint configuration $A_j(k)$ by the two change-of-coordinate transforms (Fig. 3a):

$$A_m(k) = A_h A_j(k) A_t \qquad (8)$$

where $A_m(k)$ is the measured configuration of the thumb metacarpal TCS with respect to the hand TCS at time k, A_h is the fixed transform of the hand FCS in the hand TCS, $A_j(k)$ is the functional joint configuration of the metacarpal FCS in the hand FCS at time k, and A_t is the fixed transform of the thumb metacarpal TCS in the thumb metacarpal FCS. The relation in Eq. (8) can be expanded in terms of the each transform's orientation component R and location component p:

$$A_m(k) = \begin{bmatrix} R_h & p_h \\ \vec{0} & 1 \end{bmatrix} \begin{bmatrix} R_j(k) & p_j(k) \\ \vec{0} & 1 \end{bmatrix} \begin{bmatrix} R_t & p_t \\ \vec{0} & 1 \end{bmatrix}$$
$$= \begin{bmatrix} R_m(k) & p_m(k) \\ \vec{0} & 1 \end{bmatrix}. \qquad (9)$$

We use the robotics Denavit-Hartenberg (DH) convention [see, e.g., 18] to parameterize $A_j(k)$ for the kinematic model depicted in Fig. 3b (Table I). This convention provides a framework to describe both the joint axis orientation and joint axis location, and it has been used previously to describe the non-orthogonal and non-intersecting axes of the thumb joints in recent literature [4, 11]. The FE axis z_h fixed in the hand frame is orthogonal to and intersects the PS axis, and the PS axis is orthogonal to and intersects the AA axis z_t fixed in the thumb metacarpal frame. The distance between the intersection points on the PS axis defines the separation d between the FE and AA axes, and the value of the PS rotation angle determines the skew angle between the FE and AA axes. The value for the PS rotation angle for non-singular configurations will be near 90 degrees. The general form of $A_j(k)$ is expressed in terms of the fixed separation d and the three joint angles θ_1, θ_2, and θ_3, using the abbreviated notation $c_i = \cos\theta_i$ and $s_i = \sin\theta_i$,

Input: z_h, axis orientation in hand TCS
Input: z_t, axis orientation in thumb TCS
Input: A_m, sequence of N measured transformations consisting of rotations R_m and $n \geq 1$ marker positions $p_{m1}, \ldots, p_{mn}$
Input: v, vector denoting proximal to distal direction in the hand TCS
Output: cost metric value

1: // first estimate joint angles relative to arbitrary θ_1 and θ_3 values
2: $R_h \leftarrow$ rotation of minimum angle that aligns z-axis of hand TCS to z_h
3: $R_t \leftarrow$ rotation of minimum angle that aligns z-axis of thumb TCS to z_t
4: **for** each time sample k **do**
5: $\quad R_j(k) \leftarrow R_h^{\mathrm{T}} R_m(k) R_t^{\mathrm{T}}$
6: $\quad \theta_1(k), \theta_2(k), \theta_3(k) \leftarrow$ InverseKinematics($R_j(k)$)   solution with $\theta_2(k) \geq 0$
7: **end for**
8: // update joint angles to reference configuration
9: $R_h \leftarrow R_h * Rotation(z, \mathrm{mode}(\theta_1))$
10: $R_t \leftarrow Rotation(z, \mathrm{mode}(\theta_3)) * R_t$
11: **for** each time sample k **do**
12: $\quad R_j(k) \leftarrow R_h^{\mathrm{T}} R_m(k) R_t^{\mathrm{T}}$
13: $\quad \theta_1(k), \theta_2(k), \theta_3(k) \leftarrow$ InverseKinematics($R_j(k)$)   solution with $\theta_2(k) \geq 0$
14: **end for**
15: // use orientation parameters to estimate location parameters
16: $d, p_h, p_t \leftarrow$ LeastSquaresEstimate($R_h, R_t, R_j, \theta_1, p_{m1}, \ldots, p_{mn}$)
17: // adjust sign of separation d to describe the proximal-distal relation between FE and AA axes
18: $x_h \leftarrow x$ axis of R_h
19: $d \leftarrow |d| \mathrm{sign}(v \cdot x_h)$
20: cost $\leftarrow$ CostFunction($\theta_1, \theta_2, \theta_3, d$)
21: **return** cost

Fig. 4. Pseudocode for the evaluation of a four-DoF solution family (z_h, z_t) for a given measured sequence A_m and set of n marker trajectories $(p_{m1}, p_{m2}, \ldots p_{mn})$.

TABLE I
DENAVIT-HARTENBERG PARAMETERS FOR DESCRIBING THE FUNCTIONAL CONFIGURATION OF THE CMC JOINT MODEL. THERE ARE THREE ROTATIONAL AXES WITH NO TRANSLATIONAL DEGREES OF FREEDOM. SUCCESSIVE AXES ARE MUTUALLY ORTHOGONAL, AS INDICATED BY THE LINK TWIST VALUES. THE FE AND AA AXES ARE SEPARATED BY JOINT OFFSET d ALONG THE PS AXIS WHICH IS THE MUTUAL PERPENDICULAR. THE SKEW BETWEEN THE FE AND AA AXES IS DEFINED BY THE ROTATION ANGLE θ_2 ABOUT THE PS AXIS.

link number	joint axis	joint angle θ	link length a	link twist α	joint offset d
1	FE	θ_1	0	$-\frac{\pi}{2}$	0
2	PS	θ_2	0	$\frac{\pi}{2}$	d
3	AA	θ_3	0	0	0

as:

$$A_j(k) = \begin{bmatrix} c_1 c_2 c_3 - s_1 s_3 & -c_1 c_2 s_3 - s_1 c_3 & c_1 s_2 & -ds_1 \\ s_1 c_2 c_3 + c_1 s_3 & -s_1 c_2 s_3 + c_1 c_3 & s_1 s_2 & dc_1 \\ -s_2 c_3 & s_2 s_3 & c_2 & 0 \\ 0 & 0 & 0 & 1 \end{bmatrix}. \qquad (10)$$

Overall, 13 fixed parameters specifying A_h, A_t, and d describe the CMC joint model, while the values of the three joint variables at all N time samples describe a measured motion sequence. Instead of optimizing over the high-DoF space (A_h, A_t, d) and solving for the joint angles to compute the cost metric, we can simplify the search to a four-parameter domain for (z_h, z_t) by using the measured motion A_m to solve for the remaining nine parameters and $3N$ joint variables.

2) Joint coordinate system orientation: We first consider the orientation component of the model, because the orientation R_m is independent of all location parameters, as seen from Eq. (9). The orientations of the joint axes are defined by only four numbers specifying the pair of axis directions (z_h, z_t). The FE axis z_h is the z-axis of R_h, the AA rotation axis z_t is the z-axis of R_t^{T}, and the PS axis is orthogonal to both z_h and z_t. For each pair (z_h, z_t), there is a family of solutions for the six-DoF set (R_h, R_t), where the corresponding functional joint angle sequences $(\theta_1, \theta_2, \theta_3)$ for a sequence of measured rotations $R_m(k)$ are fully defined up to a shift in the reference angle for θ_1 and θ_3 and a sign change for θ_2. The ambiguity in the sign of θ_2 is due to the fact that there are two sets of joints angles, $(\theta_1, \theta_2, \theta_3)$ and $(\theta_1 + \pi, -\theta_2, \theta_3 + \pi)$, corresponding to any single matrix $R_j(k)$.

We choose a canonical set of joint angle values from the family of solutions corresponding to a pair (z_h, z_t) by selecting positive values for θ_2 and reference configuration angles for θ_1 and θ_3 such that the modes of the observed angle sequences are zero (Fig. 4):

$$\mathrm{mode}(\theta_1) = 0 \tag{11}$$

$$\theta_2 > 0 \tag{12}$$

$$\mathrm{mode}(\theta_3) = 0. \tag{13}$$

The mode is computed by mapping the N continuous angle values to a discrete set of 5-degree intervals and selecting the center value of the interval with the maximum frequency. In effect, Eq. (11) and Eq. (13) specify the remaining two DoFs which select a single six-DoF set (R_h, R_t) from a four-DoF family defined by (z_h, z_t). The appropriate set (R_h, R_t) is computed by first estimating the joint angle sequences from an arbitrary choice of (R_h, R_t) within the (z_h, z_t) family and then shifting the reference configuration angles by the modes of the estimated sequences (Fig. 4, Lines 1–14). Using the mode of the joint angle sequence approximately centers the angle values around zero and avoids angle values near $\pm\pi$. Typically, the positive values of θ_2 selected by Eq. (12) will be near $+\frac{\pi}{2}$.

Thus, for any candidate set of axis directions (z_h, z_t) and a sequence of measured rotations $R_m(k)$, we can compute a canonical six-DoF orientation pair (R_h, R_t) and the set of three joint variable sequences $(\theta_1, \theta_2, \theta_3)$. The first part of Fig. 4 reviews this computation in pseudocode form.

3) Joint axes location parameters: The locations of the joint axes are defined by two position vectors p_h and p_t (Eq. (9)), as well as the separation distance d. The position vector of the measured transform A_m is a linear function of these location parameters, as derived from Eq. (9):

$$p_m(k) = p_h + R_h u_1(k)d + R_h R_j(k)p_t \tag{14}$$

where

$$u_1(k) = \begin{bmatrix} -\mathrm{s}_1(k) \\ \mathrm{c}_1(k) \\ 0 \end{bmatrix}. \tag{15}$$

Given a candidate set of orientations (R_h, R_t) which define the joint angle values, we can solve directly for the location values (p_h, p_t, d) that minimize marker reconstruction

error as a linear least squares problem. Each time sample k provides the following set of equations for the positions (p_{m1}, p_{m2}, p_{m3}) of the three markers on the metacarpal segment:

$$
\begin{bmatrix} p_{m1}(k) \\ p_{m2}(k) \\ p_{m3}(k) \end{bmatrix} =
$$

$$
\begin{bmatrix} I_3 & R_h u_1 & R_h R_j(k) & 0_3 & 0_3 \\ I_3 & R_h u_1 & 0_3 & R_h R_j(k) & 0_3 \\ I_3 & R_h u_1 & 0_3 & 0_3 & R_h R_j(k) \end{bmatrix} \begin{bmatrix} p_h \\ d \\ p_{t1} \\ p_{t2} \\ p_{t3} \end{bmatrix}
$$
$$\tag{16}$$

where I_3 is the 3×3 identity matrix and 0_3 is a 3×3 matrix of zeros. The measurements from all N time samples are combined in an overdetermined system of equations which is solved in a least squares manner for the 13×1 location parameter vector $(p_h, d, p_{t1}, p_{t2}, p_{t3})$. This completes the full specification of (A_h, A_t) defining the orientation and location of the CMC joint axes and in addition provides the separation distance d between the FE and AA axes.

Conceptually, the axis orientations (z_h, z_t) are defined by two bidirectional lines, but in practice the parameterization using directed vectors results in multiple equivalent solutions in the four-DoF space which differ by a sign change. For a physical interpretation of the separation distance d, we denote $d \geq 0$ when the AA axis is distal to the FE axis and $d < 0$ when the AA axis is proximal to the FE axis. The middle section of Fig. 4 (Lines 15–19) reviews this calculation in pseudocode form.

E. Data analysis

We determined individual CMC joint models from the experimental data by optimizing the cost metric defined in Eq. (7), whose three components model prior anatomic knowledge of the CMC joint. The tuning parameters were set to $\sigma_2 = 5$ degrees, $\mu_d = 5$ mm, and $\sigma_d = 5$ mm. The small value of σ_2 corresponds to small amounts of PS rotation. The positive value of μ_d reflects the anatomic joint property that the AA axis is distal to the FE axis, and the value of σ_d indicates the expected variation in the anatomically-plausible separation distances. With these values, the cost metric components are of approximately the same magnitude, as determined from sensitivity tests of the parameter values.

We also tested three other competing approaches for determining the axis orientations of an individual CMC joint. First, we consider a constant set of *in vitro* axis orientations which is applied to all individuals. Cooney et al. [5] measured the CMC axes based on *in vitro* bone surface geometry for 10 cadavers and reported the mean orientations of the trapezium axes with respect to the hand dorsum coordinate frame. We converted the reported results from Cooney et al. [5] for a fixed-axis rotation convention, where joint axes are fixed in the trapezium frame, to a moving-axis rotation convention for comparison to our model, where the AA axis is fixed in the metacarpal frame and moves relative to the trapezium. The joint coordinate system reported by Cooney et al. [5] only defines the axis orientation but not the axis locations. We will

calculate the location parameters for each individual using the joint angles corresponding to the set of constant axis directions (z_h, z_t) converted from the Cooney et al. [5] results (further described below).

Second, we test an optimization approach whose minimization cost metric is the marker trajectory reconstruction error for a three-DoF joint model. For a candidate set of joint axis directions (z_h, z_t), the full set of three joint angles and the location parameters were computed as described previously for our method. The cost for the set (z_h, z_t) is then calculated from the joint angles and location parameters as the root-mean-square (RMS) distance between the measured and predicted marker positions over all the markers and all time samples.

The third approach we tested is an optimization of the marker trajectory reconstruction error for a two-DoF joint model. We use this model to investigate how model constraints affect the optimization of reconstruction error. To perform this optimization, we computed reconstruction error as follows. After solving for the full set of three joint angles and location parameters given a pair (z_h, z_t), the value of θ_2 was fixed to the mean joint angle. The marker reconstruction error was then computed from the two-DoF joint angle values of θ_1 and θ_3, the constant value of θ_2, and the location parameters.

The optimization method used for the three optimization approaches was implemented in MATLAB (R2006a, Mathworks, Inc.; Natick, MA) using the built-in simplex optimization algorithm *fminsearch* to minimize the cost metric. The four-dimensional search domain represents the set of axis directions (z_h, z_t). The two numbers for each z-axis direction are the x and y components of an axis-angle rotation which aligns the current z-axis to the new z-axis direction. To improve the quality of the solution and address the problem of local minima, the search was initialized ten times. For each initialization, the two axis-angle rotations defining the directions (z_h, z_t) were chosen randomly from a uniform distribution of (x, y) points within a circle of radius $\frac{\pi}{2}$. This distribution corresponds to one hemisphere of possible z-axis distributions. The best overall local minimum from the ten initializations was selected as the final solution for the given data sequence. Preliminary testing on a small sample of the available data determined the choice of ten initializations to be sufficient for repeatable optimization results.

For all three optimization approaches, the optimization technique was applied separately to the two repetitions of the calibration movement. The two resulting joint models were compared in two-fold cross validation where the cost metric was evaluated on the motion of one repetition using the optimization result for (z_h, z_t) from the other repetition. The solution with the lower cross-validation cost was selected as the final single CMC model for the particular subject hand.

For each of the four approaches, the solution for (z_h, z_t) was then used to compute the corresponding joint variable values and the location parameters from the combined data set of both calibration movement repetitions. The average skew between the FE and AA axes is the mean value of the PS angle θ_2 from the recorded movement. RoM for all three joint angles was measured as the difference between the maximum and minimum values, as in Eq. (5). The RMS

marker position reconstruction error can be computed from the estimated location parameters and joint angle values. Note that for the marker reconstruction optimization approach of the two-DoF model, the value of θ_2 is only fixed to the mean joint angle for computing the cost metric, but for reporting results, the full set of varying values for θ_1, θ_2, and θ_3 is used for evaluation of the RoM, location parameters, and marker reconstruction error.

For the three optimization approaches, the mean direction of the axes z_h and z_t was calculated by representing each subject-specific direction as a point on the unit sphere and using the spherical averaging technique developed by Buss and Fillmore [19]. The results for the left hand were converted to the right hand coordinate frame, such that a single distribution of axis orientations included results for both hands of all subjects. The mean direction $\bar{z}$ was compared to the constant *in vitro* joint axis direction z_c reported by Cooney et al. [5]. Inter-subject variability is measured from the angular deviation of an individual axis orientation z relative to the mean axis orientation $\bar{z}$.

III. RESULTS

Optimizing the anatomy-based cost metric resulted in an intuitive alignment of the CMC axes due to the qualitative characteristics modeled in the cost metric (Fig. 5). The average axis directions from our proposed optimization method differed from the constant *in vitro* axis directions by 20 degrees and 35 degrees for z_h and z_t, respectively (Table II). The deviation of a subject-specific axis to the mean axis was at most 27 degrees and 53 degrees for z_h and z_t. In contrast, the optimization of marker reconstruction error for both the three-DoF and two-DoF joint models failed to consistently estimate anatomically-plausible directions. For the reconstruction optimization of a three-DoF model, the deviation of a subject-specific axis was as much as 105 and 96 degrees z_h and z_t respectively, indicating a lack of consistent axis directions. The reconstruction optimization of the two-DoF model also resulted in large maximum deviations of 105 and 95 degrees for z_h and z_t respectively, and the average location of the AA axis in the metacarpal frame differed unacceptably from z_c by 72 degrees.

For all four approaches, the resulting RoMs (Table III) decrease in order of FE, AA, and PS movement, as in previous descriptions of the functional CMC motion [1]. However, the RoMs determined from our anatomy-based optimization were the most consistent with the concept that the CMC joint is predominantly a two-DoF joint. The PS RoM was on average 23 degrees and at most 34 degrees using our approach, while for the other three approaches the average was at least 28 degrees and the maximum was at least 49 degrees. In addition, the anatomy-based optimization measured overall larger FE RoM than the other two models due to the alignment of the axis orientations to each subject's specific movement. In a comparison of the marker reconstruction optimization for a three-DoF model and two-DoF model, the constraint in the two-DoF model results in a smaller PS RoM. Since the optimization of marker reconstruction error for the three-DoF
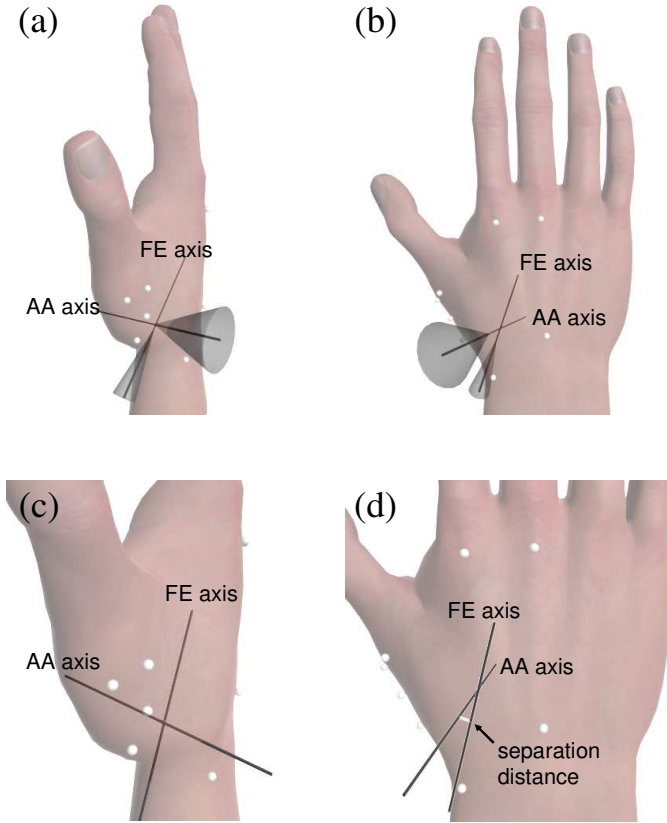
Fig. 5. (a,b) CMC joint model results for our anatomy-based optimization approach are represented by average directions of the FE axis and AA axis over 48 hands from 24 subjects. The cone denotes the mean angular deviation from the mean direction (Table II). (c,d) Close-up views of the CMC joint model for one example subject. (c) In the radial view, the separation distance between joint axes is nearly orthogonal to the page. (d) In the dorsal view, the white line highlights the separation distance between the FE and AA axis locations.

model is the least constrained with respect to possible joint angle values, for two individual thumbs the optimization result with the least reconstruction error occurred near the rotation singularities $\theta_2 = \pi$ such that the FE RoM and AA RoM were greater than 145 degrees.

The anatomy-based optimization also resulted in models where the FE axis was always proximal to the AA axis, unlike the other models which resulted in the FE axis distal to the AA axis for 10%, 35%, and 67%, respectively, of the thumbs for the constant axis orientation model, marker reconstruction optimization of the three-DoF model, and marker reconstruction optimization of the two-DoF model. Overall, for our anatomy-based approach, the separation distance between the FE and AA axes of each individual CMC joint model was 4.6 mm on average, with 1.2 mm standard deviation across all hands. The mean value of the PS angle θ_2, representing skew between the FE and AA axes, was 87 ± 17 degrees (mean $\pm$ standard deviation) from the positive flexion axis to the positive abduction axis. Average RMS reconstruction error for the calibration movement was 2.4 mm per marker, which was only slightly greater than 2.2 mm, 1.9 mm, and 2.0 mm for the constant axis orientation model, marker reconstruction optimization of the three-DoF joint model, and marker reconstruction optimization

of the two-DoF joint model, respectively.

Repeatability of the methods is measured by the difference between the optimized parameter values for the two separate repetitions of the calibration movement (Table IV). By definition, the constant axis orientation model is 100% repeatable for the axis orientations since it models zero inter- and intra-subject variability. In comparing the three optimization approaches, the resulting FE axis direction with maximum RoM estimated from our anatomy-based approach was repeatable for at least an additional 31% of the individual hands than that from either of the two marker reconstruction optimizations. The difference in repeatability of the AA axis with medium RoM was less clear with respect to the reconstruction approach for the two-DoF model. This suggests that the FE axis with maximum RoM is more well-defined than the AA axis with medium RoM. For the relative configurations of the FE and AA axes, our anatomy-based approach had the maximum repeatability of all three approaches for values of the mean θ_2 skew angle within 1 degree and the separation distance d within 0.5 mm. Overall, our optimization of the anatomy-based cost metric allowed for inter-subject variation of the joint axis directions and in addition resulted in improved intra-subject repeatability of the separation distance and skew angle between the dominant axes.

IV. DISCUSSION

Our method fits a subject-specific CMC joint model for evaluating CMC mobility with respect to axes that are aligned to an individual's particular motion. The anatomy-based cost metric reflects the preference for consistency with known CMC characteristics over purely minimizing the marker reconstruction error, which may result in anatomically-implausible parameter estimates. A convenient feature of the method is the simplified parameterization of the problem such that the pair of axis orientations (z_h, z_t) are sufficient to determine the entire joint model, including axis locations, separation distance between axes, and skew angle between axes. The low-dimensional parameterization of candidate joint models simplifies the complexity of the search space which reduces the computational expense of the optimization, and a reasonable optimum solution is found with a small number of reinitializations.

A. Description of thumb kinematics

Measurements of the functional joint angles across 48 hands from 24 subjects show that CMC mobility can be described by two dominant DoFs of FE rotation and AA rotation. However, the amount of PS rotation is not necessarily negligible given that the PS RoM for active movement was 23 degrees on average and as high as 34 degrees for one individual. Investigation of the joint angle trajectories for a subset of the measured sequences did not find that any specific part of the calibration motion consistently exhibited greater PS rotation. PS movement was present throughout the calibration movement, and the PS RoM differed by only a few degrees between the four parts. Our technique provides a way to determine the two dominant axes of rotation without precluding measurement of

TABLE II
DISTRIBUTION OF CMC FE AXIS AND AA AXIS DIRECTIONS OVER 48 HANDS OF 24 SUBJECTS FOR THE THREE OPTIMIZATION APPROACHES. WE
COMPARE THE MEAN DIRECTION FROM EACH SET OF OPTIMIZED AXES TO FIXED AXIS ORIENTATIONS DETERMINED FROM *in vitro* BONE SURFACE
GEOMETRY BY COONEY ET AL. [5]. THE MEAN AND MAXIMUM DEVIATION OF THE OPTIMIZED AXES REFLECT THE AMOUNT OF INTER-SUBJECT
VARIABILITY CORRESPONDING TO EACH MODEL.
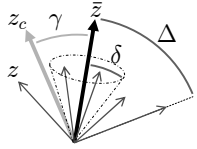
| Model | Angular deviation (degrees) from mean axis $\bar{z}$ to | | | |
| | Constant axis z_c from *in vitro* joint model, γ | | Subject-specific axis z mean δ [maximum Δ] | |
	z_h (FE)	z_t (AA)	z_h (FE)	z_t (AA)
Marker reconstruction optimization, three-DoF model	26	7	44 [105]	45 [96]
Marker reconstruction optimization, two-DoF model	40	72	38 [105]	38 [95]
Anatomy-based optimization (our method)	20	34	9 [27]	22 [53]

TABLE III
MEASURED RANGE OF MOTION FOR ACTIVE MOVEMENT OF THE CMC JOINT FOR FOUR MODELING APPROACHES: CONSTANT AXIS ORIENTATIONS FOR
ALL SUBJECTS BASED ON *in vitro* MEASUREMENTS [5], SUBJECT-SPECIFIC AXES FITTED FROM OPTIMIZING THE MARKER RECONSTRUCTION ERROR FOR
A THREE-DOF JOINT MODEL, SUBJECT-SPECIFIC AXES FITTED FROM OPTIMIZING THE MARKER RECONSTRUCTION ERROR FOR A TWO-DOF JOINT
MODEL, AND SUBJECT-SPECIFIC AXES FITTED FROM OPTIMIZING AN ANATOMY-BASED COST METRIC (OUR METHOD).

| Model | Active range of motion (degrees) mean [maximum] | | |
	θ_1 (FE)	θ_2 (PS)	θ_3 (AA)
Constant axis orientation model	69 [87]	29 [49]	46 [77]
Marker reconstruction optimization, three-DoF model	66 [182]	44 [71]	62 [164]
Marker reconstruction optimization, two-DoF model	71 [146]	28 [51]	66 [112]
Anatomy-based optimization (our method)	76 [98]	23 [34]	43 [69]

TABLE IV
REPEATABILITY OF KINEMATIC PARAMETER ESTIMATES BASED ON THE DIFFERENCE BETWEEN PARAMETER VALUES ESTIMATED FROM TWO SEPARATE
REPETITIONS OF THE ACTIVE ROM CALIBRATION MOVEMENT. THE RESULTS OF USING OUR ANATOMY-BASED COST METRIC ARE COMPARED TO
RESULTS OBTAINED FROM THE CONSTANT AXIS ORIENTATION MODEL REPORTED BY COONEY ET AL. [5] AND TWO OPTIMIZATION APPROACHES WHICH
MINIMIZE MARKER TRAJECTORY RECONSTRUCTION ERROR.

Estimated parameter	Model	Percent of hands where difference between two estimates is within		
Orientation parameters		5 degrees	10 degrees	20 degrees
z_h (FE axis) direction	Constant axis orientation model	100	100	100
	Marker reconstruction optimization, three-DoF model	8	25	38
	Marker reconstruction optimization, two-DoF model	33	58	69
	Anatomy-based optimization (our method)	65	94	100
z_t (AA axis) direction	Constant axis orientation model	100	100	100
	Marker reconstruction optimization, three-DoF model	17	27	46
	Marker reconstruction optimization, two-DoF model	31	52	67
	Anatomy-based optimization (our method)	23	54	88
		1 degree	5 degrees	10 degrees
Mean θ_2 value, defining skew between FE and AA axes	Constant axis orientation model	35	60	92
	Marker reconstruction optimization, three-DoF model	4	23	40
	Marker reconstruction optimization, two-DoF model	27	44	60
	Anatomy-based optimization (our method)	77	88	98
Location parameter		0.5 mm	1 mm	2 mm
Separation d between FE and AA axes	Constant axis orientation model	60	98	100
	Marker reconstruction optimization, three-DoF model	23	52	65
	Marker reconstruction optimization, two-DoF model	44	73	81
	Anatomy-based optimization (our method)	88	100	100

the PS RoM, as would be necessary for previous models which assume *a priori* that the joint has only two rotational DoFs.

Our non-invasive technique fits a subject-specific model to motion data which samples the entire space of *in vivo* CMC joint configurations, rather than determining the axis orientations from simplified movements restricted to, for example, only flexion or circumduction. We found that the AA axis was less well defined than the FE axis, and future studies are needed to explore whether this is explained by the anatomical joint constraints. In addition, our method can measure the average skew angle and separation distance between the FE axis and AA axis, and our estimates for both values were anatomically-plausible.

B. Crafting a reliable cost metric

Our choice of optimization cost metric components is based on anatomic CMC joint properties, rather than a minimization of only the marker trajectory reconstruction error as used in prior work [14–16]. Optimizing the reconstructed marker positions was insufficient for fitting an anatomically-meaningful model, since there may be several candidate solutions with low reconstruction error but whose corresponding joint angle values are inconsistent with functional anatomical descriptions. In addition, using the reconstruction error as the cost metric resulted in decreased repeatability of the estimated kinematic parameters (Table IV). The loss in the anatomical plausibility and repeatability corresponds to only a slight improvement in the mean RMS reconstruction error from 2.4 mm for our method to 1.9 mm in the best alternative we tested. It is possible that the small scale of the hand complicates the applicability of evaluating only marker reconstruction error to fit anatomically-meaningful joint axes, which has been successfully accomplished for other joints of the body [14–16].

Our anatomy-based approach allowed us to incorporate prior knowledge about the CMC joint to solve for anatomically-plausible joint parameters, and the results of our method do depend on the selected values of the weighting parameters used to tune the cost metric. Adjusting the weights, and thus relative magnitudes, of the cost components will bias the result toward joint models which satisfy the modeled constraints to different degrees. Our experience was that even in the reduced dimensionality of the search space, there may be several near-optimum solutions associated with each individual cost component such that an unbalanced relative weighting may not satisfy all of the constraints reasonably. For example, choosing $\sigma_2 = 10$ degrees in our sensitivity tests relaxes the constraint for small variation in the PS angle which for some subjects led to a solution where the AA and PS axes were misaligned to achieve a smaller value of f_{RoM}. The parameters of μ_d and σ_d were also critical for weighting the cost metric toward positive values of the separation distance without compromising the metrics on the joint angles. Selecting $\mu_d = 10$ mm and $\sigma_d = 5$ mm, for example, did result in larger separation distance values, but the axis orientations were misaligned for a few subjects such that the AA RoM was greater than the FE RoM or the PS RoM was greater than the AA RoM.

Given the importance of selecting appropriate weights for the optimization, the sensitivity to optimization parameters might be further investigated using Monte Carlo simulations to determine the distribution of possible parameter values. In addition, the weighting parameters in this study reflect prior knowledge of unimpaired CMC joints, and more work is needed to determine how to change the parameters and cost metric for evaluation of pathological joints.

C. Marker protocol considerations

Although our experiments used the same marker protocol for all subjects for the purpose of reporting inter-subject variability with respect to a consistent reference frame, the presented optimization framework is general and can work with any arbitrary choice of the hand TCS and thumb TCS that define the configurations of trapezium bone and thumb metacarpal bone. When using surface marker techniques, however, the marker placement should still be designed carefully to minimize systematic error due to the difference between the TCS on the skin surface and the ideal coordinate system of the bone. The quality of the optimization result is also limited by the amount of non-rigidity of the marker set.

For our experimental protocol, relative motion between the trapezium bone and the metacarpal bones or between the second and third metacarpal bones are potential sources of systematic artifacts in the TCS measurement. Skin movement relative to the bone also affects the reliability of the TCS measurement. We tried to reduce these artifacts by spacing out marker positions over the segments and directing subjects to avoid motion of other hand joints during the calibration movement. The motion artifacts may be interpreted as additional rotation or translation of the coordinate frames, but our results suggest that the optimization method finds anatomically-plausible orientations of the joint axes which can be used to reasonably evaluate the joint RoM. Further investigation is required to determine the robustness to additional skin artifacts resulting from more functionally-relevant calibration movements which include motion of the other hand joints.

Another point of caution is that the cost metric component modeling the variance of the PS angle and the least squares estimate of the location parameters are sensitive to outliers in the marker trajectories. The perturbation due to outliers was reduced by omitting any time samples with occluded markers rather than manually filling the trajectory gaps. This was possible since our method requires only a set of multiple CMC joint configurations that is not necessarily a continuous motion trajectory. In addition, the least squares estimate of the location parameters uses the positions of multiple markers on the thumb metacarpal instead of only the single marker denoting the thumb TCS frame origin. While this does not account for systematic error affecting the entire marker set, we are able to estimate the parameters describing the location and separation between joint axes which are consistent with the CMC joint anatomy even in the presence of skin deformation.

D. Extensions for further study

Although we use one specific DH parameterization of the motion transform A_j, the method can be adapted for

other representations of three sequential rotations about the coordinate system axes. In all cases the orientation of the joint axes are independent of the position parameters of the joint model. Regardless of the order of coordinate axes rotation used to parameterize R_j, one column vector of R_h denotes the first axis of rotation and one vector in R_t^{T} denotes the third axis of rotation. Thus, the reduced four-DoF parameterization for the joint axes can be used with other rotation conventions.

Our method solves for a set of joint axes which are aligned to an individual's pattern of motion, and it is suitable for objectively and non-invasively measuring the CMC joint mobility from the three joint angle RoMs. In addition, the method can be used in a skeletal-fitting procedure to automatically construct a subject-specific kinematic hand model for applications such as haptic interfaces, virtual rehabilitation systems, and computer graphics. The developed framework is not limited to surface marker techniques, as it can accommodate any experimental technology which measures the relative transform between a TCS defining the trapezium frame and a TCS defining the thumb metacarpal bone frame. A potential avenue for further research is to use the optimization method together with medical imaging techniques which measure the bone configurations directly to investigate the relationship between the axes derived from the motion pattern and the axes defined by bone surface geometry. The estimation of the joint axes orientation and location parameters may then be used for periodic evaluation of the bone surface wear, soft tissue deterioration, and changes in thumb mobility.

References

[1] I. A. Kapandji, *The Physiology of the Joints*, 2nd ed. Edinburgh: E & S Livingstone, 1970, vol. 1.
[2] T. Imaeda, K.-N. An, and W. P. Cooney, "Functional anatomy and biomechanics of the thumb." *Hand Clin.*, vol. 8, no. 1, pp. 9–15, 1992.
[3] A. Hollister, W. L. Buford, L. M. Myers, D. J. Giurintano, and A. Novick, "The axes of rotation of the thumb carpometacarpal joint." *J. Orthop. Res.*, vol. 10, no. 3, pp. 454–460, May 1992.
[4] V. J. Santos and F. J. Valero-Cuevas, "Reported anatomical variability naturally leads to multimodal distributions of Denavit-Hartenberg parameters for the human thumb." *IEEE Trans. Biomed. Eng.*, vol. 53, no. 2, pp. 155–163, February 2006.
[5] W. P. Cooney, M. J. Lucca, E. Y. Chao, and R. L. Linscheid, "The kinesiology of the thumb trapeziometacarpal joint." *J. Bone Joint Surg. Am.*, vol. 63, no. 9, pp. 1371–1381, December 1981.
[6] J. H. Coert, H. G. van Dijke, S. E. Hovius, C. J. Snijders, and M. F. Meek, "Quantifying thumb rotation during circumduction utilizing a video technique." *J. Orthop. Res.*, vol. 21, no. 6, pp. 1151–1155, November 2003.
[7] X. Zhang, P. Braido, S. W. Lee, R. Hefner, and M. Redden, "A normative database of thumb circumduction in vivo: center of rotation and range of motion." *Hum. Factors*, vol. 47, no. 3, pp. 550–561, 2005.
[8] L. Chèze, N. Doriot, M. Eckert, C. Rumelhart, and J. J. Comtet, "[In vivo cinematic study of the trapezometacarpal joint] (in French)," *Chir. Main.*, vol. 20, no. 1, pp. 23–30, February 2001.
[9] P. Cerveri, E. D. Momi, N. Lopomo, G. Baud-Bovy, P. Pajardi, and G. Ferrigno, "In-vivo estimation of the kinematic parameters of the trapezio-metacarpal joint using surface markers," *J. Biomech.*, vol. 39, no. Supplement 1, p. S82, 2006.
[10] F. J. Valero-Cuevas, M. E. Johanson, and J. D. Towles, "Towards a realistic biomechanical model of the thumb: the choice of kinematic description may be more critical than the solution method or the variability/uncertainty of musculoskeletal parameters." *J. Biomech.*, vol. 36, no. 7, pp. 1019–1030, July 2003.
[11] D. J. Giurintano, A. M. Hollister, W. L. Buford, D. E. Thompson, and L. M. Myers, "A virtual five-link model of the thumb." *Med. Eng. Phys.*, vol. 17, no. 4, pp. 297–303, June 1995.
[12] J. A. Katarincic, "Thumb kinematics and their relevance to function." *Hand Clin.*, vol. 17, no. 2, pp. 169–174, May 2001.
[13] P. W. Brand and A. Hollister, *Clinical Mechanics of the Hand*, 3rd ed. St. Louis, MO: C.V. Mosby, 1993, pp. 121–122.
[14] H. J. Sommer and N. R. Miller, "A technique for kinematic modeling of anatomical joints," *J. Biomech. Eng.*, vol. 102, no. 4, pp. 311–317, 1980.
[15] A. van den Bogert, G. D. Smith, and B. M. Nigg, "In vivo determination of the anatomical axes of the ankle joint complex: an optimization approach." *J. Biomech.*, vol. 27, no. 12, pp. 1477–1488, 1994.
[16] J. A. Reinbolt, J. F. Schutte, B. J. Fregly, B. I. Koh, R. T. Haftka, A. D. George, and K. H. Mitchell, "Determination of patient-specific multi-joint kinematic models through two-level optimization." *J. Biomech.*, vol. 38, no. 3, pp. 621–626, 2005.
[17] C. M. Bishop, *Pattern Recognition and Machine Learning*. New York, NY: Springer, 2006, pp. 21–28.
[18] M. W. Spong, S. Hutchinson, and M. Vidyasagar, *Robot Modeling and Control*. Hoboken, NJ: John Wiley & Sons, Inc., 2006, ch. 3.2.
[19] S. R. Buss and J. P. Fillmore, "Spherical averages and applications to spherical splines and interpolation," *ACM Trans. Graph.*, vol. 20, no. 2, pp. 95–126, April 2001.

Lillian Chang received the M.S. degree in robotics from Carnegie Mellon University in 2006. She is currently working toward the Ph.D. degree at the Robotics Institute at Carnegie Mellon University. Her research interests include biomechanical modeling of the hand, dexterous manipulation in humans, and control of anthropomorphic robotic manipulators. She received a National Science Foundation Graduate Research Fellowship in 2004.

Nancy Pollard is an Associate Professor in the Robotics Institute and the Computer Science Department at Carnegie Mellon University. She received her PhD in Electrical Engineering and Computer Science from the MIT Artificial Intelligence Laboratory in 1994, where she performed research on grasp planning for articulated robot hands. Before joining CMU, Nancy was an Assistant Professor and part of the Computer Graphics Group at Brown University. She received the NSF CAREER award in 2001 for research on 'Quantifying Humanlike Enveloping Grasps' and the Okawa Research Grant in 2006 for "Studies of Dexterity for Computer Graphics and Robotics."